Peer-reviewed version available at *Nanomaterials* **2019**, *9*, 89; doi:10.3390/nano9010089

Article

Supramolecular Organogels Based on *N*-Benzyl, *N'*-Acylbispidinols

Alexey V. Medved'ko[1], Alexander I. Dalinger[1], Vyacheslav N. Nuriev[1], Vera S. Semashko[1], Andrei V. Filatov[2], Alexander A. Ezhov[3,4], Andrei V. Churakov[5], Judith A. K. Howard[6], Andrey A. Shiryaev[7,8], Alexander E. Baranchikov[1,5], Vladimir K. Ivanov[5,9] and Sergey Z. Vatsadze[1]*

[1] Faculty of Chemistry, Lomonosov Moscow State University, 119991 Moscow, Russian Federation; szv@org.chem.msu.ru
[2] Zelinsky Institute of Organic Chemistry, Russian Academy of Sciences, 119991 Moscow, Russian Federation
[3] Faculty of Physics, Lomonosov Moscow State University, 119991 Moscow, Russian Federation
[4] Topchiev Institute of Petrochemical Synthesis, Russian Academy of Sciences, 119991 Moscow, Russian Federation
[5] Kurnakov Institute of General and Inorganic Chemistry of the Russian Academy of Sciences, 119991 Moscow, Russian Federation
[6] Department of Chemistry, University of Durham, Durham, DH1 3LE, UK
[7] Frumkin Institute of Physical Chemistry and Electrochemistry, Russian Academy of Sciences, 119071 Moscow, Russian Federation
[8] Institute of geology of ore deposits, petrography, mineralogy and geochemistry, Russian Academy of Sciences, 119017 Moscow, Russian Federation
[9] Faculty of Material Science, Lomonosov Moscow State University, 119991 Moscow, Russian Federation
* Correspondence: szv@org.chem.msu.ru ; Tel.: +7-903-748-7892

Abstract: The acylation of unsymmetrical *N*-benzylbispidinols in aromatic solvents without external base led to formation of supramolecular gels, which possess different thickness and stability depending on the substituents in *para*-positions of benzylic group and nature of acylating agent as well as on the nature of the solvent used. Structural features of the native gels as well as of their dried forms were studied by complementary techniques including FT IR- and ATR-spectroscopy, AFM, TEM, SEM, SAXS. Structures of the key crystalline compounds were established by X-ray diffraction. Analysis of obtained data allowed speculating on the crucial structural and condition factors that governed the gel formation. The most important factors were: (i) absence of base, either external or internal; (ii) presence of HCl; (iii) presence of carbonyl and hydroxyl groups to allow hydrogen bonding; (iv) presence of two (hetero)aromatic rings at both sides of the molecule. The hydrogen bonding involving amide carbonyl, hydroxyl at 9th position and, very probably, ammonium N-H+ and Cl- anion appear to be responsible for the formation of infinite molecular chains required for the first step of gel formation. Subsequent lateral cooperation of molecular chains into fibers occured, presumably, due to the aromatic pi-pi-stacking interactions. sc-CO_2 drying of the gels gave rise to aerogels morphology different from that of air dried samples.

Keywords: organic nanomaterials**,** bispidines; supramolecular gels; SEM, TEM, AFM study; X-ray diffraction; FT IR-spectroscopy; ATR-spectroscopy; SAXS

1. Introduction

Positron emission tomography (PET) is one of widely used molecular imaging methods enabling early and high-resolution diagnostics of various diseases including oncological, neurological and cardiovascular [1,2]. There is a growing interest in the field of new radiopharmaceuticals (RP) with non-conventional PET radionuclides, e.g. ^{86}Y (14.7 h), ^{89}Zr (78.4 h), ^{64}Cu (12.7 h), etc. in recent years [3–5]. Among other, ^{64}Cu is one of the most promising isotopes for the PET usage because it possesses the smallest average energy of positrons, and its half-life allows delivery to local clinics [6,7]. Unlike conventional PET radionuclides (^{15}O, ^{13}N, ^{11}C, ^{18}F), incorporation of metal isotope in RP

requires use of poly/multifunctional chelating agents that should form covalent bonds with various biomolecules/vectors possessing high specificity and selectivity towards certain targets [5], [8–11]. 3,7-Diazabicyclo[3.3.1]nonanes (hereafter called bispidines) are one of the privileged scaffolds in medicinal chemistry [12] due to the number of advantages, e.g. (i) high basicity and solubility in water and/or organic solvents [13,14]; (ii) ability to diverse functionalization including chiral derivatives [15–20]; (iii) deeply studied conformational features which allow application of some rigid conformation [21–23]. Our recent works have shown potential of using the bispidine scaffolds for design of inhibitors of serine proteases [24,25]. At the same time, bispidines are well-known ligands with high affinity to Cu(II) and some other bivalent metals [26–29]. Therefore, we focus on creating new potent ligands for ^{64}Cu PET based on number of unsymmetrically substituted bispidine-9-ols. During our work with ligands for serine proteases it was necessary to find a way to insert bulky groups into pockets of the active site [24,25]. The acylation reaction is one of the obvious ways to functionalize the secondary amine group in *N*-benzylbispidinols; the resulting *N*-benzyl, *N'*-acylbispidinols allow subsequent transformations like reduction of amide group or removal of the protecting benzylic group followed by diverse functionalization of the formed secondary amine. In the course of our work we have discovered an interesting phenomenon, namely, formation of gels during the acylation of *N*-benzylbispidinols in benzene.

The supramolecular gels belong to broad family of supramolecular materials [30]. Since the beginning of investigation of supramolecular gels in mid-1990s, this area attracts significant interest due to many exciting and unique features exhibited by this soft matter [31,32] [33–41]; see also special issue of Beilschtein Journal of Organic Chemistry [42] and Tetrahedron Symposium-in-Print Number 130 [43]; vol. 256 of Topics in Current Chemistry [44]; special issue of Gels [https://www.mdpi.com/journal/gels/special_issues/supramol_gels], and a monograph [45]. The uniqueness of supramolecular gels in manifested in their intrinsic stimuli-responsive nature [46]. Their properties span from high porosity [47] to mechanically robust materials [48]; they could form unexpected composites with polymers [39] and photopatterned materials [49]; they are known for their self-sorting properties [50] and could be used as photophysical materials with unique properties [51,52]. Even they could be exploited as pollutant removers [53] and for programmed cell growth [54].

The synthesis of a family of unsymmetrically *N,N'*-disubstituted bispidine-9-ols derivatives, gelling properties of their HCl salts and possible explanation of such behavior will be discussed in this manuscript.

2. Materials and Methods

Synthesis. General methods.

Compounds **1**-**3** were synthesized according to procedures described in [24,55,56].

A solution of acyl halide (1 eq.) in dry benzene was added dropwise to a suspension of bispidine **3** (1 eq.) in dry benzene under vigorous stirring. In most cases the gel-like substance started to form after first several drops of the acyl halide solution. Then the mixture was refluxed under vigorous stirring for 3.5 hours. To obtain the product as the hydrochloride, the resulting gelatinous mass (precipitate or colloidal solution) was centrifuged for 10-15 minutes (6000 rpm) or filtered on a Schott filter (por.40) and then air dried with subsequent drying on rotary evaporator. The free base was isolated from the aqueous solution of the formed solid hydrochloride by treatment with sodium bicarbonate (3 eq.) and characterized (SI p. 2–6). For study of native benzenogels the reaction mixture was allowed to cool down to room temperature (*vide infra*).

Supercritical carbon dioxide drying was performed using home-made rig (volumes 5 mL or 80 mL, the details see [57,58]). In typical experiments the working pressure and temperature were 80-90 bar and 40-50 ^{0}C, respectively.

Small-angle X-ray scattering and diffraction (SAXS). SAXS patterns were acquired using dedicated small-angle diffractometer SAXSess (Anton Paar, Austria) employing monochromatic Cu-*Kα*1 radiation (1.5412 A). The samples were placed into standard glass capillary 1.5 mm in diameter and sealed. The measurements were performed in vacuum; scattered radiation was recorded using 2D Imaging plates.

Fourier-transform infrared (FTIR) spectra were acquired using SpectrumOne spectrometer coupled with AutoImage microscope (Perkin Elmer). The samples were placed on gold mirror and spectra represent superposition of absorption (dominant) and reflectance components.

Atomic force microscopy (AFM). AFM measurements were made by scanning probe microscope NTEGRA Prima (NT-MDT). Semicontact mode was used. The amplitude of the "free air" probe oscillations was from 20 to 25 nm (peak-to-peak). High-resolution noncontact/semicontact silicon AFM probes "Golden" NSG01 series (NT-MDT) were used. Topography, feedback error signal and phase difference were registered simultaneously for the samples. The samples were prepared by drying the sol on silicon wafers.

Transmission electron microscopy (TEM). TEM images were obtained using transmission electron microscope LEO912 AB OMEGA (Carl Zeiss, Germany) operating at 100 kV voltage. Samples were prepared by drying the sol droplets placed on copper grids coated by FormvarTM film.

Scanning electron microscopy (SEM). SEM images were obtained using Carl Zeiss NVision 40 workstation at 1 kV accelerating voltages using secondary electron (SE2) detector. The preparation of the samples was the same as for the AFM measurements.

X-Ray. Experimental intensities were measured on Bruker SMART 1K (for **4cb** and **2c**) and Bruker SMART APEX II diffractometers (for **4cb**, **3c**, **1b**, **4da** and 5,7-dimethyl-1,3-diazaadamantan-6-one) using graphite monochromatized Mo-*Kα* radiation (λ= 0.71073 Å) in ω-scan mode. Absorption corrections based on measurements of equivalent reflections were applied. The structures were solved by direct methods and refined by full matrix least-squares on F^2 with anisotropic thermal parameters for all non-hydrogen atoms (except solvent benzene molecule in **4da**) [59]. In **1b** and **4da** all hydrogen atoms were placed in calculated positions and refined using a riding model. As for the structures **4cb**, **2c**, **3a** and **1b** all protons were added geometrically and refined using a riding model while all hydroxy- and amino - hydrogens were located from difference Fourier synthesis and refined isotropically. Finally, in **3c** and 5,7-dimethyl-1,3-diazaadamantan-6-one all protons were found from difference map and their positional and thermal parameters were refined. The crystals of **4cb** and **1b** were racemically twinned with domain ratios 0.79/0.21 and 0.76/0.24, respectively. X-ray diffraction studies were performed at the Centre of Shared Equipment of IGIC RAS. The crystallographic data have been deposited with the Cambridge Crystallographic Data Centre as supplementary publications (for CCDC numbers see Table S3). This information may be obtained free of charge from the Cambridge Crystallographic Data Centre via www.ccdc.cam.ac.uk/data_request/cif .

3. Results

Compounds **1-3** were prepared according to protocols from [24,55,56]: the stereoselective ring opening in salts **1** leads to unsymmetrically substituted bispidinols **2;** deformylation of the later gives rise to secondary amino alcohols **3** (Scheme 1).

Preprints (www.preprints.org) | NOT PEER-REVIEWED | Posted: 12 December 2018 doi:10.20944/preprints201812.0149.v1

Peer-reviewed version available at Nanomaterials 2019, 9, 89; doi:10.3390/nano9010089

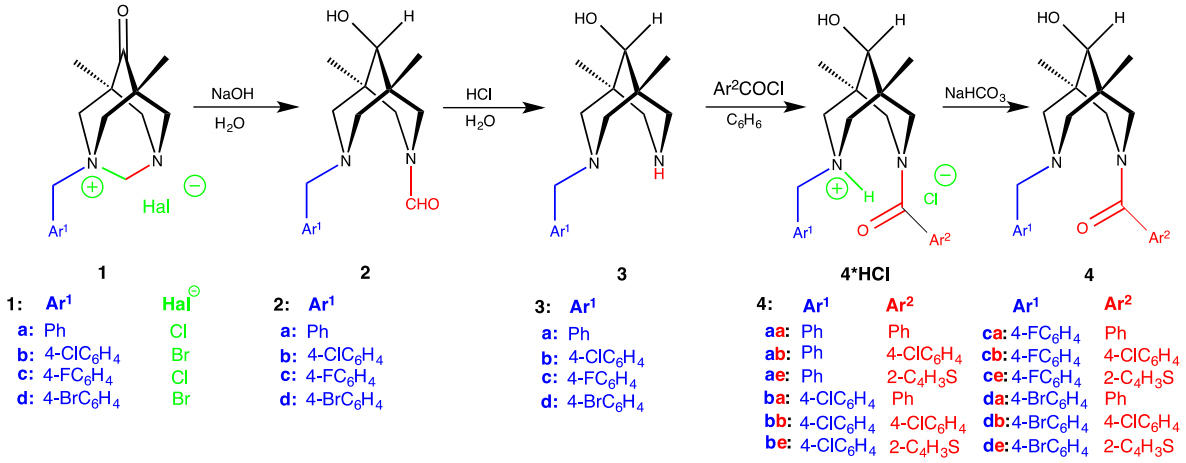

Scheme 1. Synthetic routes to the target amides **4**.

The next step, acylation of secondary amine group in **3**, is straightforward due to presence in the same molecule of a tertiary amine group which would work as an internal base to accept released HCl. It is expected that the resulting salts **4*HCl** should precipitate from the reaction mixture making the isolation easier. Indeed, the tertiary amine group worked as the internal base during the acylation, but unexpectedly, instead of the precipitation the acylation of molecules **3** in benzene in most cases (except for **4aa**, **4ba** and **4ca**) led to formation of opaque to almost transparent gel-like materials - very viscous substances with eventual presence of crystalline admixtures (see Figures S1-S7). Similar results were obtained when we used nitrobenzene, ethoxybenzene or mesitylene (in this case the least stable gels if any were produced) instead of benzene for the synthesis of **4ab*HCl** and **4ae*HCl**.

The target amides **4** were finally obtained by gentle base treatment of the salts **4*HCl** (SI p. 2–6). It was found that choice of the base is crucial to obtain the amides **4**: using of strong base like alkali lead to de-acylation instead of formation of target amino-amides. Presumably, this is due to a spatial proximity of amino lone pair and amide function. Finally, we were able to isolate and characterize 12 new amino-amides **4** differing by substituents Ar^1 and Ar^2 (see Scheme 1).

In order to understand structural features of the gels with general formulae **benzene@4*HCl** several physical-chemical methods providing information about various structural levels of supramolecular gels [30–32,60,61] were applied: – molecular (X-ray diffraction, IR-spectroscopy), nano (SAXS, SEM, TEM, AFM) and macroscopic scales (IR- and NMR-spectroscopy, SAXS, DLS, DSC, POM, rheology). Some of the applied methods failed to provide useful information. For example, we were not able to get reasonable results from NMR-spectroscopic titration of solution of **3** by acyl chloride solution since all signals appeared to be quite broad. Rheological studies applied to sample **benzene@4ce*HCl** showed that this is indeed a gel [62] but no quantitative information emerged (Table S1-S2, Figure S8-S9).

In order to understanfd possible mechanisms of the intermolecular interactions that would lead to a gel formation, we applied the single-crystal X-ray technique to those samples that were crystalline. Chemical connectivity scheme for structurally characterized samples **4cb**, **2c**, **3a**, **3c** and **4da*HCl** is presented on Scheme 2a while their molecular structures are shown in Figures S10-S14. Selected geometrical features are listed in Table 1. Main geometrical parameters of the bispidine skeleton in all studied compounds are close to the values reported and discussed for numerous bispidines and their salts in [63] and references cited therein.

Preprints (www.preprints.org) | NOT PEER-REVIEWED | Posted: 12 December 2018 doi:10.20944/preprints201812.0149.v1

Peer-reviewed version available at Nanomaterials 2019, 9, 89; doi:10.3390/nano9010089

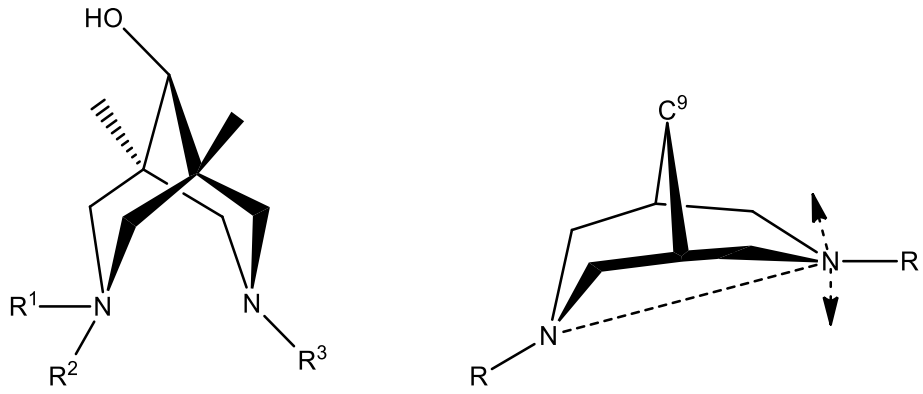

a **b**

Scheme 2. Chemical connectivity scheme for structurally characterized samples (a). The distances and deviations are discussed in text (b).

In all presented cases both piperidine cycles of bicyclic skeleton adopt chair conformation with involuntarily shortened N…N separations (see Table 1). In all five bispidine structures benzyl substituted nitrogen atoms (NBz) are almost tetrahedral with the sum of C-NBz-C angles ranging from 330.0 to 332.1°. Benzyl substituents always occupy axial positions with respect to six-membered piperidine cycles (*exo-* to the concave surface of eight-membered cycle). Of interest, hydroxyl groups at C9 positions are oriented in the same direction as the benzyl substituents. As expected, amido nitrogen atoms in **2c**, **3c**, and **4da*HCl** are almost planar due to their sp^2 nature and do not participate in hydrogen bonding. In contrast, secondary amine N atoms in **3a** and **3c** are tetrahedral with sum of angles nearly equal to 325°. Their hydrogen atoms are *endo*-oriented due to intramolecular hydrogen bonding.

The most intriguing feature of the bispidine derivatives is the conformational flexibility of both piperidine cycles. In general they can adopt chair-chair, chair-boat or boat-boat conformations [22,64]. Search in the Cambridge Structural Database (CSD, ver. 5.39, Feb 2018) [65] for structures of neutral organic flexible bispidine derivatives with sp^3- hybridized carbon atoms within eight-membered cycle produced 121 entries (136 molecules). Several additional structures with additional fused rigid cycles were rejected. . Examination of of nitrogen-nitrogen separation distribution reveals that widely used N…N distance is an inappropriate parameter for conformational analysis of bispidines. In close proximity to intermediate point (half-chair arrangement with one almost planar N atom) significant shifts of nitrogen atom (perpendicular to the main plane of the cycle) does not lead to noticeable changes in N…N distances (Scheme 2b). Therefore, mutual distribution of C9…N distances was analysed (Figure 1). Regions corresponding to chair-chair and chair-boat conformations are clearly separated on this scatterplot. The chair-chair arrangement dominates: 87 vs. 49 cases. Interestingly, in crystalline state boat-boat conformation is absent. Thus, other criteria should be used to distinguish chair-chair and chair-boat conformations: namely, the absolute value of the difference between C9…N distances (Figure S18). The approximate value 0.17 Å may be used as a threshold between these conformations.

In the structures **4cb**, **3c** and **4da** one of the two nitrogen atoms bear H atom available for hydrogen bonding. Of interest that in all cases these atoms are involved in strong ***intra***molecular hydrogen

Preprints (www.preprints.org) | NOT PEER-REVIEWED | Posted: 12 December 2018 doi:10.20944/preprints201812.0149.v1

Peer-reviewed version available at Nanomaterials 2019, 9, 89; doi:10.3390/nano9010089

bonding NH…N. Obviously such hydrogen bonding is assisted by conformational preorientation of the bispidine scaffold.

Thus, all five bispidinols contain just one "active" hydroxyl hydrogen atom suitable for formation of ***inter***molecular hydrogen bonds. Additionally, all these molecules contain several acceptors of hydrogen bond at the opposite side, promoting formation of the H-bonded chains. Actually, such chains formed by OH…O=C or OH…N bonds were observed in the structures of neutral bispidinols **4cb**, **2c**, **3a** and **3c** (Figures 3–6). In contrast, the structure of salt **4da*HCl** contains insular 0D hydrogen bonded motif due to OH…Cl hydrogen bond (Figure S14).

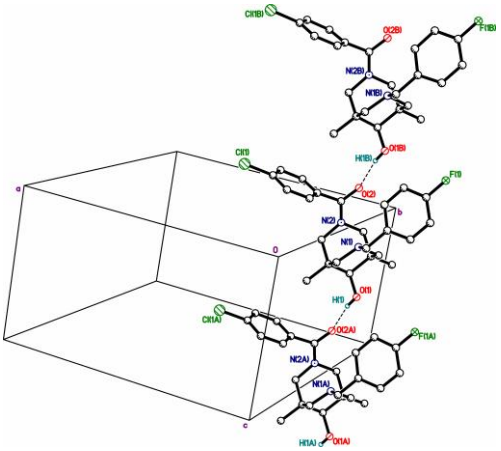

Figure 1. Hydrogen-bonded chains in the structure **4cb**.

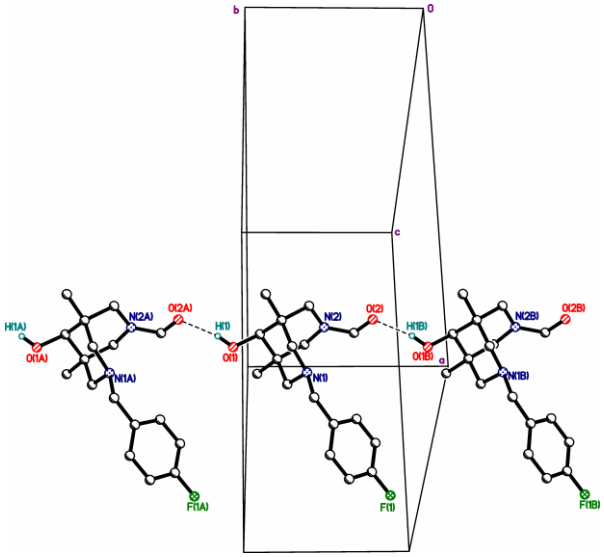

Figure 2. Hydrogen-bonded chains in the structure **2c**.

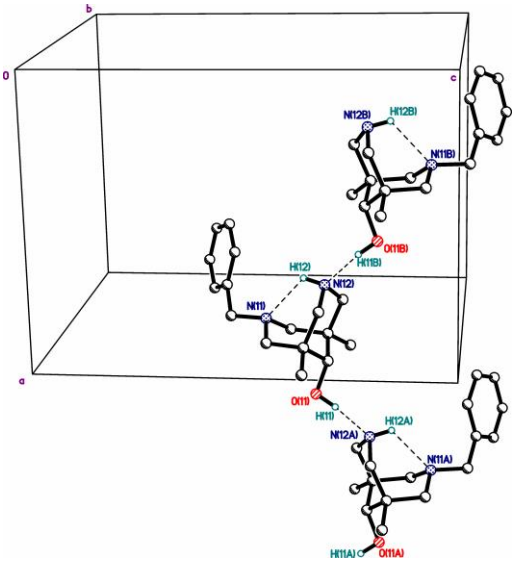

Figure 3. Hydrogen-bonded chains in the structure **3a**.

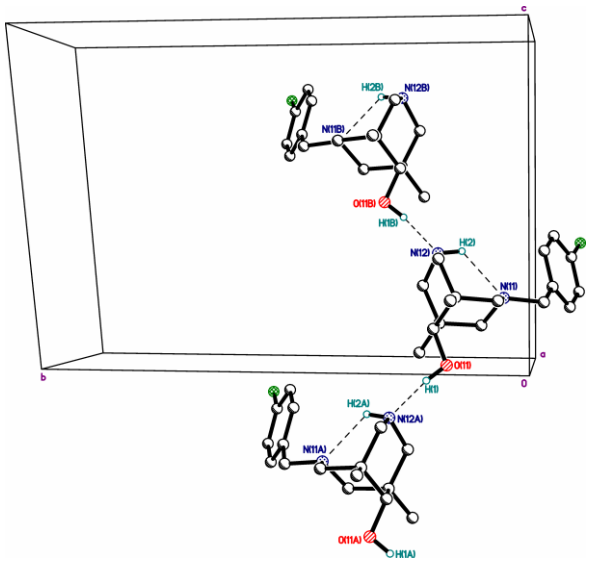

Figure 4. Hydrogen-bonded chains in the structure **3c.**

It should be noted, that **3c** is isostructural with its chlorine analogue LEFFIN (**3b**) [66].

Table 1. Selected geometric parameters for bispidines **4cb**, **2c**, **3a**, **3c**, **4da**.

	4cb	2c	3a	3c	4da*HCl
R1, R2	p-$FC_6H_4CH_2$-, —	p-$FC_6H_4CH_2$-, —	$C_6H_4CH_2$-, —	p-$FC_6H_4CH_2$-, —	p-$BrC_6H_4CH_2$-, H
R3	p-ClC6H4C(=O)-	-CH(=O)	H	H	C6H4C(=O)-
C-OH	1.423(3)	1.472(6)*	1.4195(12)	1.4178(12)	1.416(12)
av N-Cendo**	1.469(3)	1.458(3)	1.4695(15)	1.4691(14)	1.458(14)
NBz-C**	1.465(3)	1.471(3)	1.4653(14)	1.4658(13)	1.505(13)
N-CO**	1.339(3)	1.331(3)	—	—	1.375(13)
Σ C-NBz-C***	330.3	330.0	331.4	331.9	332.1
Σ C-Namid-C***	359.4	359.5	—	—	353.7
Σ ang NH***	—	—	325.0	325.8	—
X, O…X ******	=O, 2.784(3)	=O, 2.665(5)	R2HN, 2.7250(12)	R2HN, 2.7157(12)	Cl-, 3.049(10)
N…Nintra*******	2.825(3)	2.830(4)	2.8372(13)	2.8309(13)	2.790(14)

* for major component of disorder

** - average distances between nitrogen and carbon atoms (N-Cendo – between secondary amine nitrogen atoms and skeleton carbon atoms; NBz-C – between benzyl substituted nitrogen atoms and skeleton carbon atoms; N-CO – between amide nitrogen atoms and carbonyl carbon atoms).

*** - the sum of C-N-C angles (NBz – benzyl substituted nitrogen atom; Namid – amide nitrogen atom; NH – secondary amine nitrogen atom)

**** - length of hydrogen bonds

***** - intramolecular distance between nitrogen atoms

The structure **1c** comprises both ketone and its bis-diol forms. Molecular structures of the diazaadamantane derivatives **1c** and **1c+H_2O** are shown on Figures S5 and A6. Main geometrical features of the diazaadamantane scaffold in both compounds are close to those found for hydrochloride of the parent compound [63]. Notably, this is only the third known example of cocrystallization of ketone and its hydrate [67,68]. Surprisingly, the conformations of both forms are very close to each other. In **1c+H_2O** the diol form is stabilized by hydrogen bonding with adjacent chlorine anions and water molecules (Figure A6). This hydrogen-bonded system is finite and this structure represents 0D network. It should be noted that bezylation of one of the nitrogens in 5,7-dimethyl-1,3-diazaadamantan-6-one (X-ray-derived structure shown at Figure S4) leads to

inequivalence of CH_2-N bonds in both **1c** and **1c+H_2O**: the one connected to N+ became longer (1.546/1.565 A) than the initial one in the starting diazaadamantanone (1.466 A), whist the second bond becames slightly shorter (1.422/1.437 A). This is a consequence of the $n_N - \sigma^*_{N\text{-}C}$ anomeric type electronic interaction already mentioned in [69].

The infinite hydrogen-bonded chains in solid-state structures is a common motif for **2c, 3c, 4cb**. While for the amine **3c** the secondary nitrogen lone pair serves as a hydrogen bond acceptor, in amides **2c** and **4cb** carbonyl oxygens play this role. The structure of the salt **4da*HCl** differ dramatically, since in it two types of intermolecular hydrogen bonds can be distinguished. The first one bounds protonated tertiary amine hydrogen and carbonyl oxygen of the adjacent centrosymmetrically linked molecule forming the dimers. Each organic molecule is also linked to chloride-anion by the second intermolecular hydrogen bond involving the hydroxyl hydrogen at the position 9, which serves as a hydrogen bond donor like in **2c, 3c, 4cb**.

On the base of these findings for the dried materials we could tentatively suggest that the main structural motif that links molecules into the 1D supramolecular polymer within the supramolecular gel is the hydrogen bond between hydroxyl at position 9 and the hydrogen bond donor, which could be either halogenide-anion or carbonyl oxygen atom. The involvement of the hydroxyl and carbonyl groups in hydrogen bonding is confirmed by FT IR spectra of the native gels **benzene@4ce*HCl** and **benzene@4de*HCl** (Figure S25).

It should be stressed here that upon removal of benzene and ethoxybenzene the gel structure undergoes irreversible changes clearly seen in carbonyl and hydroxyl/NH regions of IR-spectra (Figure 7). These changes indicate heavy structural rearrangement of the gel which leads to the insolubility of the dried sample even in hot benzene, which was attempted to prepare a gel from the solid **4*HCl**. This could be explained as follows: removal of the solvent moves previously loosely packed molecular chains into close proximity with formation of stronger inter chain attractive interactions; another explanation could be found in the changes in intermolecular H-bonding (see below in Discussion).

Preprints (www.preprints.org) | NOT PEER-REVIEWED | Posted: 12 December 2018 doi:10.20944/preprints201812.0149.v1

Peer-reviewed version available at Nanomaterials 2019, 9, 89; doi:10.3390/nano9010089

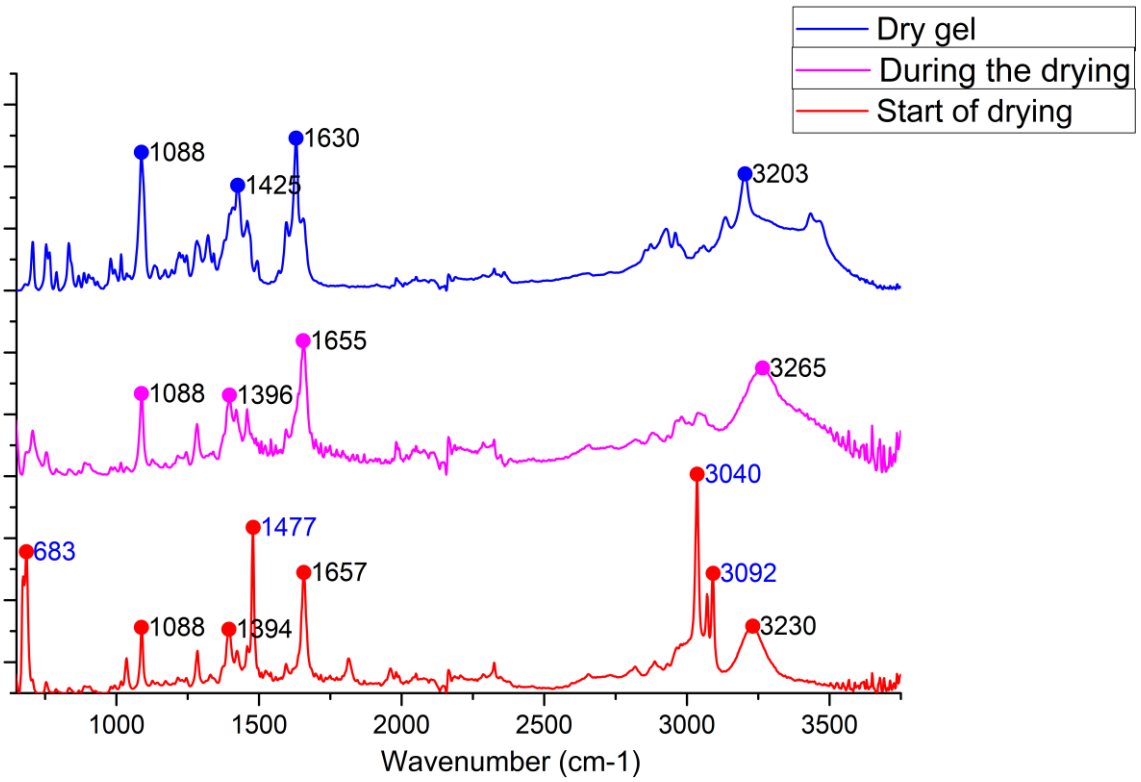

Figure 5. The changes in ATR-spectra of **4ab** during solvent removal. Benzene peaks are shown in blue. See text for details.

Nanoscale level of organization of xerogels of type **4*HCl** obtained by direct benzene evaporation was studied by AFM, SEM and TEM (Figure 8, Figures S20-S23). The data clearly show existence of long and thin nanofibers as a main structural motif of the xerogels, which is typical for supramolecular gels [32]. In some cases the nano-crystalline additives are observed. In some extreme cases width of the nanofibers is less than 100 nm.

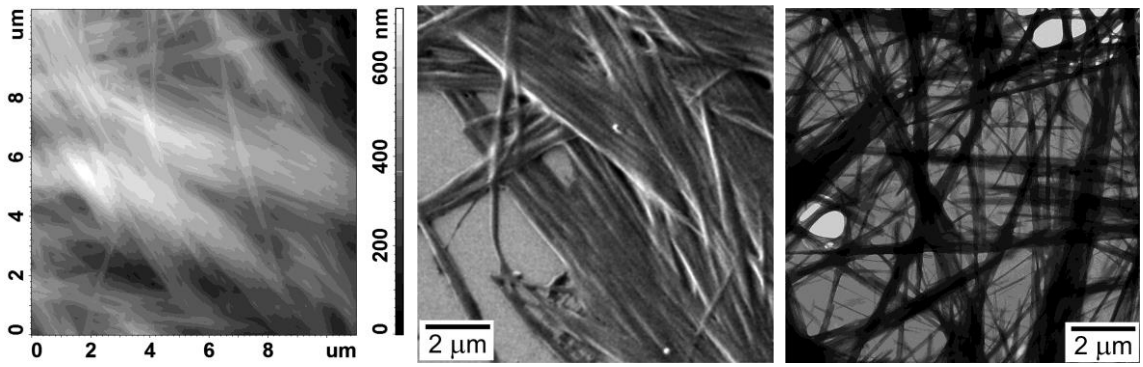

Figure 6. AFM, SEM and TEM images for the dried gel **benzene@4ce*HCl**.

The sample of benzenogel **benzene@4cb*HCl** was subjected to different procedures of the solvent removal.

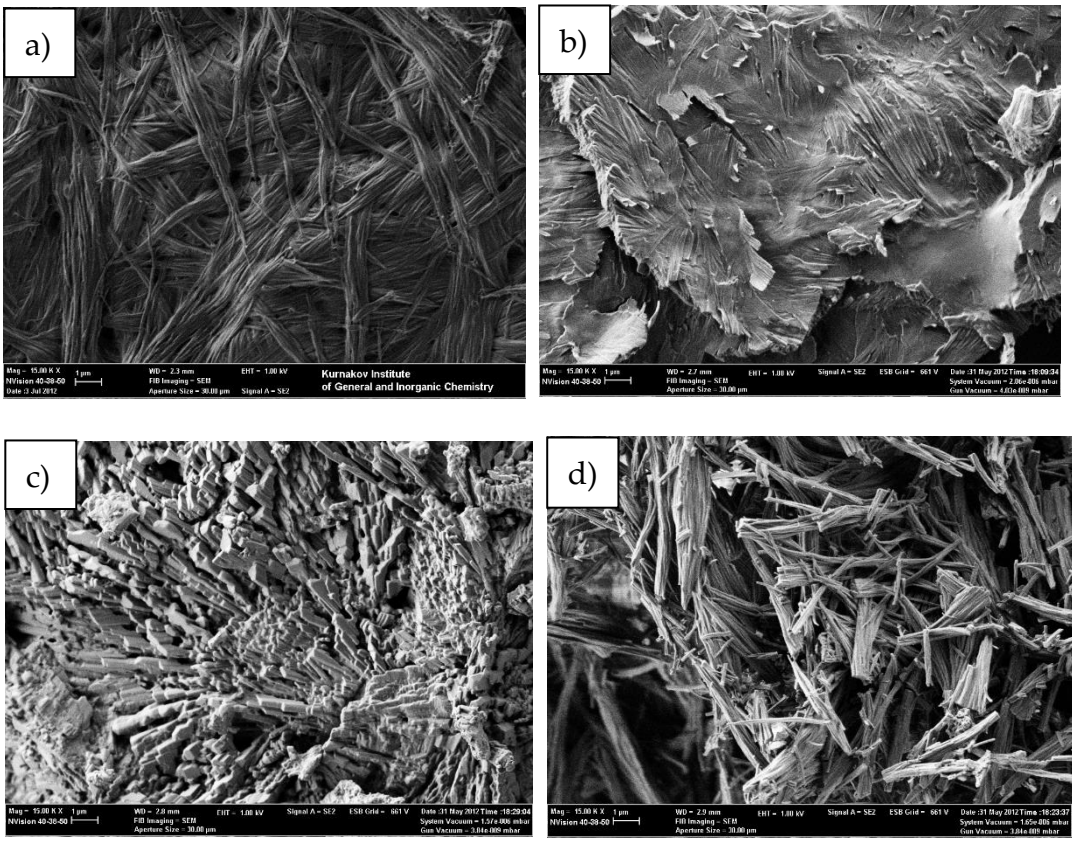

Figure 7. SEM micrographs of dry gel samples made by different methods of solvent removal from **benzene@4cb*HCl**: bulk xerogel (a), gel coated on the glass surface (b); liquid CO_2 washing (c); sc-CO_2 washing (d). Scale bar is 1 micrometer.

The drying regime drastically affects the microstructure of the gels. Figure 9 shows scanning electron microscopy images of **benzene@4cb*HCl** gels dried under different conditions. Drying under ambient conditions results in dense structures consisting from strongly interwoven and partially conglutinated fiber-like particles (Figures 9a,b). Drying in supercritical CO_2 resulted in a loose structure possessing lower aggregation degree of individual fibers (Figure 9d). Presumably the difference is due to the contribution of capillary forces. The drying under ambient conditions (xerogels) results in strong coalescence of the particles upon removal of liquid benzene and movement of menisci into the sample monolith. The supercritical drying almost levels the capillary forces effects and results in loose unaggregated monoliths. Chemical composition of the **benzene@4cb*HCl** xerogel sample is in agreement with its chemical structure: indeed, the sample contains Cl and F.

Unusual structures were formed upon washing of the gel by liquid CO_2 with subsequent solvent removal (Figures 9c). Fiber-like structure of the gel looks almost disrupted, and the sample consists of strongly coalesced particles with crystal-like shape, some particles are even faceted. Such an appearance may be due to partial dissolution of the substance in liquid CO_2 followed by re-crystallization and fast desorption of CO_2 from the sample surface resulting in disruption of fibers and formation of dendrite-like particles. The same observations were found for samples prepared from ethoxebenzene (Fig. S24)

Investigation of the xerogel sample using back-scattered electron detector (BSE-mode) (Figure 10) reveals inclusions of a secondary phase with density notably higher than that of the matrix. This finding is in agreement with POM data (Figure S7). This could be explained by the formation of some nano-crystalline domains within the amorphous gel fibers.

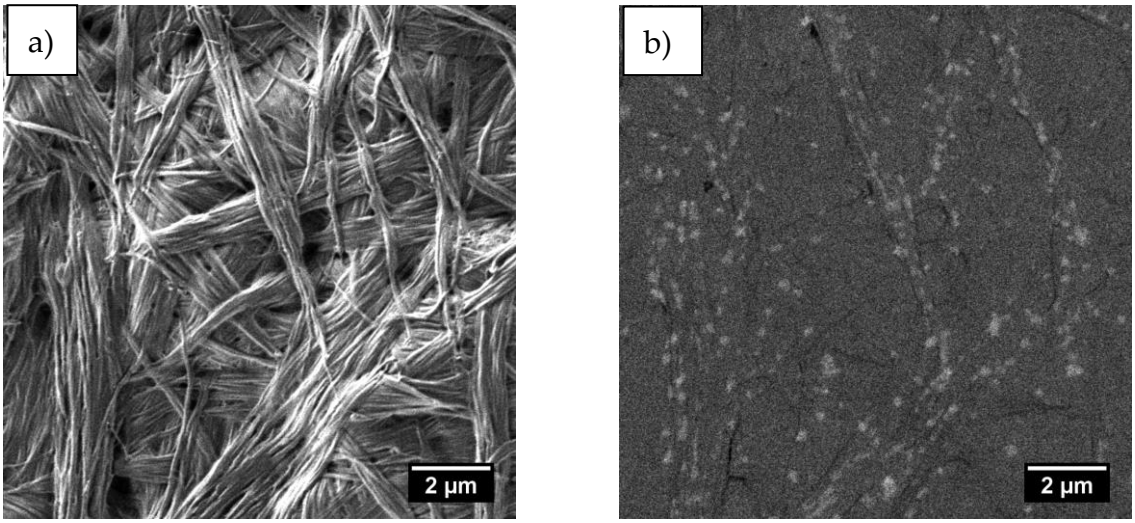

Figure 8. SEM micrographs of **benzene@4cb*HCl** xerogel sample obtained for the same area by SE2 (a) and BSE (b) detectors. Scale bar is 2 μm.

Similar differences were observed upon drying **benzene@4ce*HCl** sample under ambient conditions and in supercritical CO_2 (Figure 11).

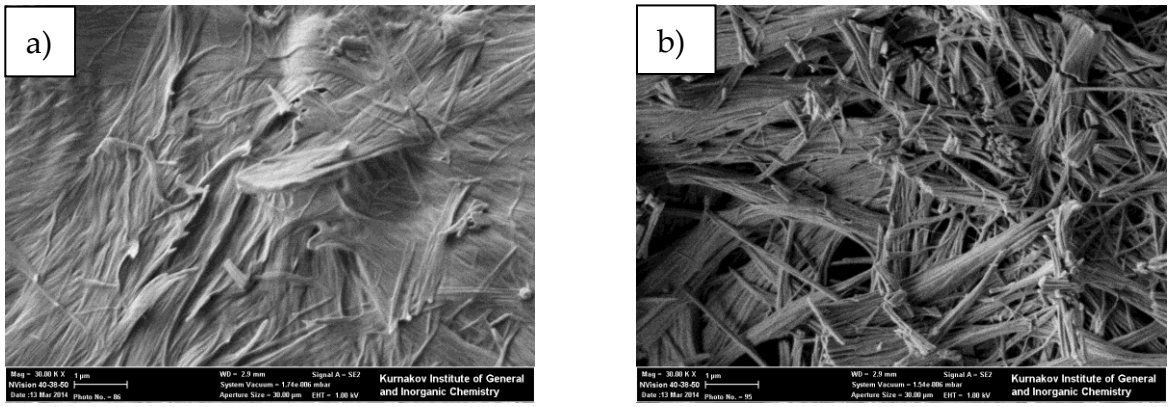

Figure 9. SEM micrographs of dry gel samples made by different methods of solvent removal from **benzene@4ce*HCl:** direct air-drying (a), sc-CO2 drying (b). Scale bar is 1 μm.

The nanoscale structure of the gels leads to highly heterogeneous spatial distribution of electron density reflected by intense Small-angle X-ray scattering (SAXS) caused by scatterers larger than 60 nm. The samples **benzene@4ce*HCl** and **benzene@4de*HCl** also possess crystallographic ordering with interlayer spacings of 2.47, 1.16 and 0.75 nm (**benzene@4ce*HCl**) and 2.4+2.7 (double peak), 1.16, 0.75 nm. (**benzene@4de*HCl**) (Figure 12).

Peer-reviewed version available at Nanomaterials 2019, 9, 89; doi:10.3390/nano9010089

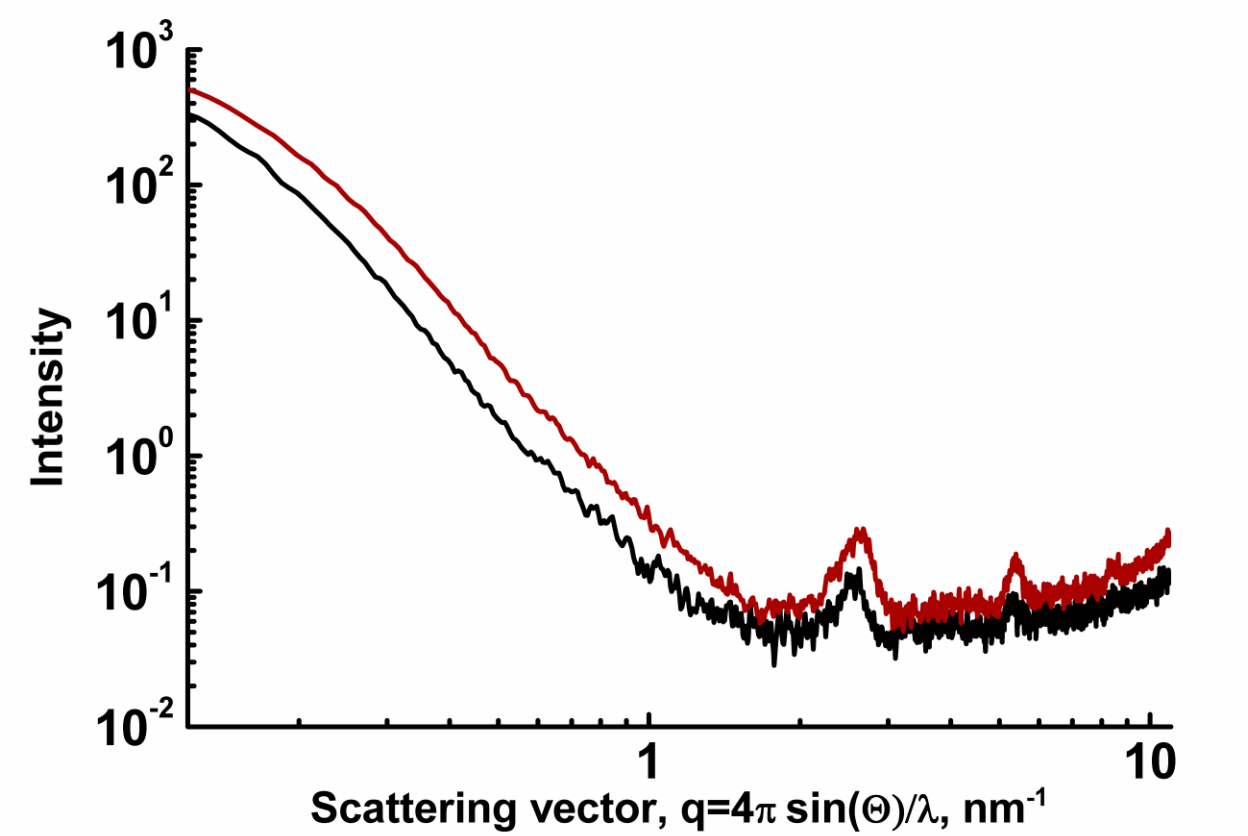

Figure 10. Small-angle X-ray scattering patterns of samples **benzene@4ce*HCl** (red) and **benzene@4de*HCl** (black).

Close similarity in scattering patterns of two different samples undoubtedly indicate the similar nano- and macrostructural organization of benzenogels based on N-benzyl, N'-acyl bispidinols. The existence of the crystallographic ordering might be a result of ordering of gelator molecules within chains, fibers and bundles. It could also point out to the presence of nano-crystalline domains within the whole gel-like material.

4. Discussion

In previous sections we have shown that acylation of secondary amines **3** in benzene by acyl chlorides led to the formation of supramolecular gels of general formulae **benzene@4*HCl**. Before we start to speculate on the structural features of new materials, some additional information and data should be taken into account:

- gels are formed only during the acylation of secondary amines of *N*-benzylbispidine-9-ols, but not upon purging the HCl gas through the solution/suspension of isolated amino-amides **4** in benzene;
- during the removal of benzene from the gel the later undergoes some irreversible structural rearrangements which lead to the further insolubility of dried material in benzene;
- the gels are formed neither in the presence of the external base (for example, triethylamine), nor from the chloroanhydrides of picolinic acids (beta or gamma) or pyrazole-contaning acid chlorides;
- removal of chloride anion by the action of aqueous silver nitrate destroys the supramolecular gel;
- the gels are not formed upon alkylation (for example, by benzylchloride);

Preprints (www.preprints.org) | NOT PEER-REVIEWED | Posted: 12 December 2018 doi:10.20944/preprints201812.0149.v1

Peer-reviewed version available at Nanomaterials 2019, 9, 89; doi:10.3390/nano9010089

- the gels are formed only from aromatic (benzoic, *para*-chlorobenzoic acid) or heteroaromatic (2-thiophencarboxylic acid) acid chlorides, but not with use of aliphatic reagents (acetylchloride, chloroanhydride of cyclopropanecarboxylic acid);
- the gels are formed also in nitrobenzene, ethoxybenzene and mesitylene at elevated temperatures (nearly 100°C), but their stability depends on the substituents at acylating agents (SI p. 6 – 9).

All these data indicate that for the formation of supramolecular gel in our systems one needs: (i) proton (in the form of protonated tertially amino-group, which was found in the crystal of **4da*HCl**); (ii) chloride-anion (obviously, to form hydrogen bonds with N-H+, like in **4da*HCl**, or O-H, like in **1c+H₂O**); (iii) carbonyl group (obviously, to form infinite chains via hydrogen bonds with O-H, like those found in the crystal structure of **4cd** or **2c**); (iv) two aromatic substituent at both nitrogen atoms of the bispidine scaffold (presumably, to form lateral intermolecular bonding via π–π-stacking interactions).

Combination of all features mentioned above allows us to formulate the following mechanism of gel formation upon acylation of amines **3** (Scheme 3). Possible participation of H-bonded supramolecular polymers like those found in crystals of **3a** or **3c** is not discussed here for simplicity, although they could play some role in the beginning of the process.

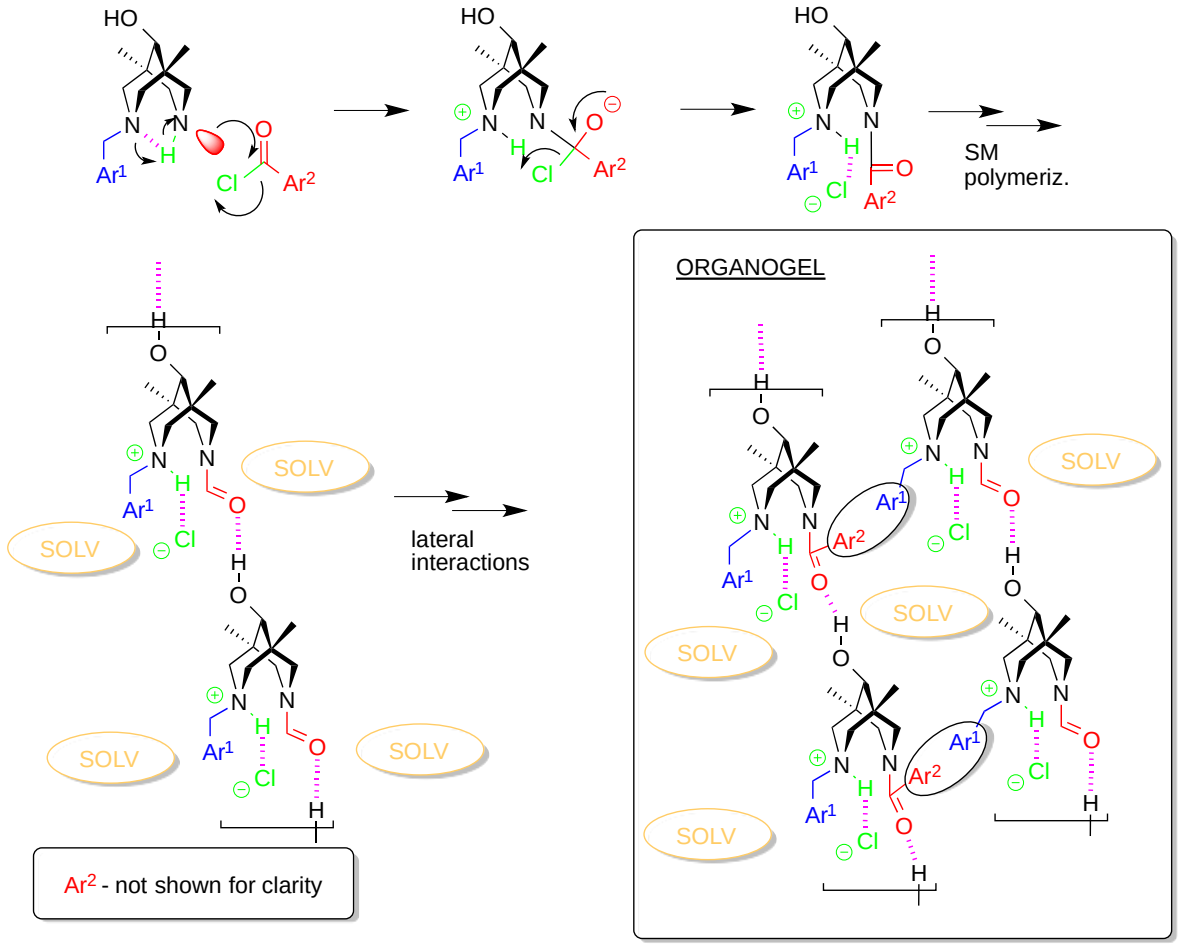

Scheme 3. Schematic representation of possible way of formation of gels.

Scheme 3 accounts for all of the factors and features mentioned above. Indeed, all the required items are presented in the scheme and all play crucial role for the process of gel formation. At the moment we lack enough data to reveal mechanism of the aggregation of species of molecular size, schematically shown as a result of supramolecular polymerization that includes both the formation of H-bonds and π–π-stacks. The role of solvent in these processes is also unclear, but we could

Preprints (www.preprints.org) | NOT PEER-REVIEWED | Posted: 12 December 2018 doi:10.20944/preprints201812.0149.v1

Peer-reviewed version available at Nanomaterials 2019, 9, 89; doi:10.3390/nano9010089

assume the importance of the donor/acceptor properties of the aromatic solvent as well as its steric demands. Indeed, in nitrobenzene the strongest gel is formed when pi-donor thiophene acid chloride is applied. On contrast, the sterically demanding mesitylene forms least stable gels among this row of solvents: nitrobenzene, mesitylene, benzene, ethoxybenzene.

At the same time, assuming that the benzenogel building block shown on Scheme 3 indeed appeared during the gel formation, we could explain the changes of gel structure during the solvent removal, see Scheme 4. At the molecular/supramolecular level one expects the change in the main H-bonded motif from polymeric chain to discreet dimers of type [**4da*HCl**]$_2$. This explains the evolution of IR-spectra during the solvent evaporation: both OH/NH and C=O regions displays remarkable changes of the corresponding vibrations (*vide supra*). Obviously such changes will affect the nano/macro level of the gel organization, and various methods of the solvent removal will result is different morphologies of the final solids.

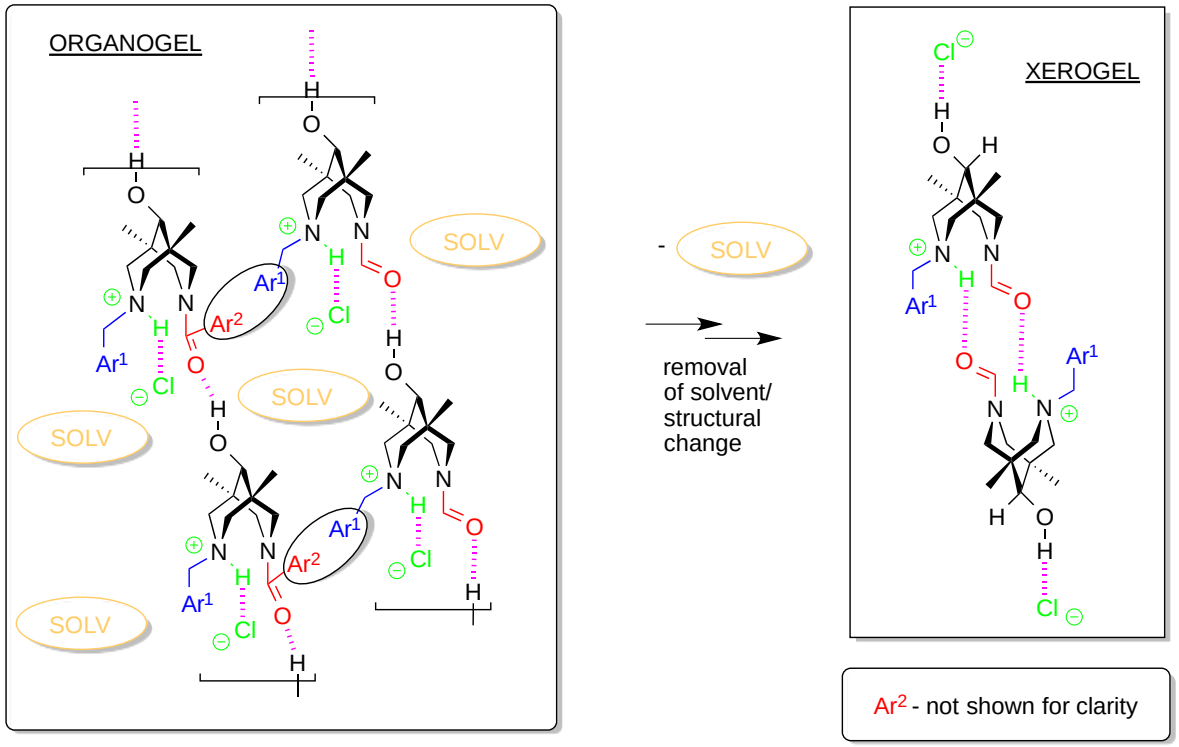

Scheme 4. Schematic representation of the structural changes upon solvent removal from benzenogel.

5. Conclusions

In conclusion, we have discovered new family of low molecular weight gelators (LMWG) based on the HCl salts of unsymmetrical *N*-benzyl, *N'*-acyl bispidinols. The first example of the aerogel preparation from supramolecular gel is reported. The scope and limitations of the new class of LMWG is a subject of our current studies. The investigation of copper and zirconium complexes of new ligands and their gel forms for possible PET applications is also on our agenda.

Supplementary Materials: The following are available online at www.mdpi.com/link, Figure S1: Photo of **4ae*HCl** in nitrobenzene, Figure S2: Photo of **4ae*HCl** in ethoxybenzene, Figure S3: Photo of **4ae*HCl** in mesitylene, Figure S4: Photo of **4ab*HCl** in nitrobenzene, Figure S5: Photo of **4ab*HCl** in ethoxybenzene, Figure S6: Photo of **4ab*HCl** in mesitylene, Figure S7: POM photomicrography, Figure S8: Dependence of viscosity on shear rate, Figure S9: Dependence of the loss and accumulation modules on angular frequency, Figure S10: Molecular structure of **4cb**, Figure S11: Molecular structure of **2c**., Figure S12: Molecular structure of **3a**, Figure S13: Molecular structure of **3c**, Figure S14: Molecular structure of **4da*HCl*(C$_6$H$_6$)$_2$**, Figure S15: Hydrogen-bonded finite motif in the structure **1c+H2O**, Figure S16: Molecular structure of

5,7-dimethyl-1,3-diazaadamantan-6-one, Figure S17: The structures a) and b) of ketone and its diol form in the crystal 1c, Figure S18: Scatterplot of C9…N separations in structures of neutral organic flexible bispidines, Figure S19: Histogram of absolute differences between C9…N separations, Figure S20: TEM micrograph of 4bc*HCl,Figure S21-S23: AFM micrograph of **4bc*HCl**, Figure S24: SEM micrographs of dry gel samples made by different methods of solvent removal from **ethoxybenzene@4ae*HCl**, Figure S25: FT IR spectra of the native gels **benzene@4de*HCl** and **benzene@4ce*HCl**, Table S1: Dependence of shear rate on viscosity, Table S2: Dependence of the loss and storage moduli on angular frequency, Table S3: Crystal data, data collection, structure solution and refinement parameters for **4cb**, **2c**, **3a**, **3c**, **1b**, **5,7-dimethyl-1,3-diazaadamantan-6-one** and **4da**.

Acknowledgments: The X-ray diffraction studies were carried out within the State Assignment on Fundamental Research to the Kurnakov Institute of General and Inorganic Chemistry.
Authors would like to thank Dr. S.S. Abramchuk (Nesmeyanov Institute of Organoelement Compounds, Russian Academy of Sciences) for assistance in TEM measurements. Authors thank: Dr. A.Ryabchun for his help with POM studies; Dr. A. Romanchuk for her help in DLS studies; E.Raitman for her help in DSC studies; V. Maidannik for his help in rheology investigation.
This work was supported by Russian Science Foundation (grant №16-13-00114).

Author Contributions: S.Z.V., A.V.M. and V.N.N. conceived and designed the experiments; A.V.M., A.I.D., V.N.N., V.S.S. and A.V.F. performed the experiments; V.N.N. contributed to NMR study; V.S.S. contributed to ATR; A.V.F. contributed to POM, DLS and DSC; A.A.E. contributed to AFM; A.V.C. and J.A.K.H. contributed to X-Ray; A.A.S. contributed to SAXS and FT IR; A.E.B. contributed to SEM; S.Z.V, A.I.D., A.A.E, A.V.C and V.K.I. wrote the paper; S.Z.V. contributed to general management.

References

1. Hendel, R. C.; Kimmelstiel, C. *Cardiology Procedures*; 2017; ISBN 978-1-4471-7288-8.
2. Vatsadze, S. Z.; Eremina, O. E.; Veselova, I. A.; Kalmykov, S. N.; Nenajdenko, V. G. ^{18}F-Labelled catecholamine type radiopharmaceuticals in the diagnosis of neurodegenerative diseases and neuroendocrine tumours: Approaches to synthesis and development prospects. *Russian Chemical Reviews* **2018**, *87*, doi:10.1070/RCR4752.
3. Jødal, L.; Le Loirec, C.; Champion, C. Positron range in PET imaging: Non-conventional isotopes. *Physics in Medicine and Biology* **2014**, *59*, 7419–7434, doi:10.1088/0031-9155/59/23/7419.
4. Holland, J. P.; Williamson, M. J.; Lewis, J. S. Unconventional Nuclides for Radiopharmaceuticals. *Molecular Imaging* 2010, *9*, 1–20.
5. Schubiger, A. P.; Lehmann, L.; Friebe, M. *PET Chemistry (Ernst Schering Research Foundation Workshop 62)*; 2007; ISBN 3540326235.
6. Paterson, B. M.; Donnelly, P. S. Macrocyclic Bifunctional Chelators and Conjugation Strategies for Copper-64 Radiopharmaceuticals. In *Advances in Inorganic Chemistry*; Elsevier Inc., 2016; Vol. 68, pp. 223–251 ISBN 9780128035269.
7. Lee, S. gyu; Gangangari, K.; Kalidindi, T. M.; Punzalan, B.; Larson, S. M.; Pillarsetty, N. V. K. Copper-64 labeled liposomes for imaging bone marrow. *Nuclear Medicine and Biology* **2016**, *43*, 781–787, doi:10.1016/j.nucmedbio.2016.08.011.
8. Comba, P.; Kerscher, M.; Rück, K.; Starke, M. Bispidines for radiopharmaceuticals. *Dalton Transactions* **2018**, *47*, 9202–9220, doi:10.1039/c8dt01108g.
9. Comba, P.; Jermilova, U.; Orvig, C.; Patrick, B. O.; Ramogida, C. F.; Rück, K.; Schneider, C.; Starke, M. Octadentate Picolinic Acid-Based Bispidine Ligand for Radiometal Ions. *Chemistry - A European Journal* **2017**, *23*, 15945–15956, doi:10.1002/chem.201702284.
10. Medved'Ko, A. V.; Egorova, B. V.; Komarova, A. A.; Rakhimov, R. D.; Krut'Ko, D. P.; Kalmykov, S. N.; Vatsadze, S. Z. Copper-Bispidine Complexes: Synthesis and Complex Stability Study. *ACS Omega* **2016**, *1*, 854–867, doi:10.1021/acsomega.6b00237.
11. Stephan, H.; Walther, M.; Fahnemann, S.; Ceroni, P.; Molloy, J. K.; Bergamini, G.; Heisig, F.; Muller, C. E.; Kraus, W.; Comba, P. Bispidines for Dual Imaging. *Chemistry - A European Journal* **2014**, *20*, 17011–17018, doi:10.1002/chem.201404086.
12. Tomassoli, I.; Gündisch, D. Bispidine as a Privileged Scaffold. *Current topics in medicinal chemistry* **2016**, *16*, 1314–1342, doi:10.2174/1568026615666150915111434.
13. Comba, P.; Morgen, M.; Wadepohl, H. Tuning of the properties of transition-metal bispidine complexes by variation of the basicity of the aromatic donor groups. *Inorganic Chemistry* **2013**, *52*, 6481–6501, doi:10.1021/ic4004214.
14. Toom, L.; Kütt, A.; Kaljurand, I.; Leito, I.; Ottosson, H.; Grennberg, H.; Gogoll, A. Substituent Effects on the Basicity of 3,7-Diazabicyclo[3.3.1]nonanes. *The Journal of Organic Chemistry* **2006**, *71*, 7155–7164, doi:10.1021/jo0604991.
15. Breuning, M.; Steiner, M. Chiral Bispidines. *Synthesis* **2008**, *2008*, 2841–2867, doi:10.1055/s-2008-1067241.
16. Asymmetric Aldol Reaction Using New Bispidine Catalysts. *Synfacts* **2008**, *2008*, 0647–0647, doi:10.1055/s-2007-1072754.
17. Haridas, V.; Sadanandan, S.; Sharma, Y. K.; Chinthalapalli, S.; Shandilya, A. Bispidine as a secondary structure nucleator in peptides. *Tetrahedron Letters* **2012**, *53*, 623–626, doi:10.1016/j.tetlet.2011.11.112.
18. Zhang, Y. C.; Gao, J. Y.; Shi, N. Y.; Zhao, J. Q. Synthesis of Chiral Tridentate Ligands Embodying the Bispidine Framework and their Application in the Enantioselective Addition of Diethylzinc to

Aldehydes. *Advanced Materials Research* **2011**, *396–398*, 1236–1243, doi:10.4028/www.scientific.net/AMR.396-398.1236.

19. Stucchi, M.; Lesma, G. Split- Ugi Reaction with Chiral Compounds: Synthesis of Piperazine- and Bispidine-Based Peptidomimetics. *Helvetica Chimica Acta* **2016**, *99*, 315–320, doi:10.1002/hlca.201500505.
20. Rossetti, A.; Landoni, S.; Meneghetti, F.; Castellano, C.; Mori, M.; Colombo Dugoni, G.; Sacchetti, A. Application of chiral bi- and tetra-dentate bispidine-derived ligands in the copper(<scp>ii</scp>)-catalyzed asymmetric Henry reaction. *New Journal of Chemistry* **2018**, *42*, 12072–12081, doi:10.1039/C8NJ01930D.
21. Zefirov, N. S.; Palyulin, V. A. Topics in Stereochemistry. *Topics in Stereochemistry* **1991**, *20*, 171.
22. Vatsadze, S. Z.; Krut'ko, D. P.; Zyk, N. V.; Zefirov, N. S.; Churakov, A. V.; Howard, J. A. First 1H NMR observation of chair-boat conformers in bispidinone system. Molecular structure of 3,7-diisopropyl-1,5-diphenyl-3,7-diazabicyclo-[3.3.1]nonane-9-one. *Mendeleev Communications* **1999**, *9*, XXVI–XXVII.
23. Palyulin, V. A.; Emets, S. V; Chertkov, V. A.; Kasper, C.; Schneider, H. J. Conformational switching of 3,7-diacyl-3,7-diazabicyclo[3.3.1]nonanes by metal binding and by solvent changes. *European Journal of Organic Chemistry* **1999**, *2*, 3479–3482, doi:10.1002/(SICI)1099-0690(199912)1999:12<3479::AID-EJOC3479>3.0.CO;2-H.
24. Kudryavtsev, K. V.; Shulga, D. A.; Chupakhin, V. I.; Sinauridze, E. I.; Ataullakhanov, F. I.; Vatsadze, S. Z. Synthesis of novel bridged dinitrogen heterocycles and their evaluation as potential fragments for the design of biologically active compounds. *Tetrahedron* **2014**, *70*, 7854–7864, doi:10.1016/j.tet.2014.09.009.
25. Vatsadze, S. Z.; Shulga, D. A.; Loginova, Y. D.; Vatsadze, I. A.; Wang, L.; Yu, H.; Kudryavtsev, K. V. Computer modeling of ferrocene-substituted 3,7-diazabicyclo[3.3.1]nonanes as serine protease inhibitors. *Mendeleev Communications* **2016**, *26*, 212–213, doi:10.1016/j.mencom.2016.04.011.
26. Comba, P.; Kerscher, M.; Schiek, W. Bispidine Coordination Chemistry. *Progress in Inorganic Chemistry* **2007**, *55*, 613–704, doi:10.1002/9780470144428.ch9.
27. Comba, P.; Jakob, M.; Rück, K.; Wadepohl, H. Tuning of the properties of a picolinic acid-based bispidine ligand for stable copper(II) complexation. *Inorganica Chimica Acta* **2017**, doi:10.1016/j.ica.2017.08.022.
28. Comba, P.; Hunoldt, S.; Morgen, M.; Pietzsch, J.; Stephan, H.; Wadepohl, H. Optimization of Pentadentate Bispidines as Bifunctional Chelators for 64 Cu Positron Emission Tomography (PET). *Inorganic Chemistry* **2013**, *52*, 8131–8143, doi:10.1021/ic4008685.
29. Atanasov, M.; Comba, P.; Martin, B.; Müller, V.; Rajaraman, G.; Rohwer, H.; Wunderlich, S. DFT models for copper(II) bispidine complexes: Structures, stabilities, isomerism, spin distribution, and spectroscopy. *Journal of Computational Chemistry* **2006**, *27*, 1263–1277, doi:10.1002/jcc.20412.
30. Amabilino, D. B.; Smith, D. K.; Steed, J. W. Supramolecular materials. *Chemical Society Reviews* 2017, *46*.
31. Vieira, V. M. P.; Hay, L. L.; Smith, D. K. Multi-component hybrid hydrogels – understanding the extent of orthogonal assembly and its impact on controlled release. *Chem. Sci.* **2017**, doi:10.1039/C7SC03301J.
32. Hirst, A. R.; Escuder, B.; Miravet, J. F.; Smith, D. K. High-tech applications of self-assembling supramolecular nanostructured gel-phase materials: from regenerative medicine to electronic devices. *Angewandte Chemie (International ed. in English)* **2008**, *47*, 8002–18, doi:10.1002/anie.200800022.
33. Draper, E. R.; Adams, D. J. Low-Molecular-Weight Gels: The State of the Art. *Chem* 2017, *3*.
34. Weiss, R. G. The past, present, and future of molecular gels. What is the status of the field, and where is it going? *Journal of the American Chemical Society* 2014, *136*.

35. Sangeetha, N. M.; Maitra, U. Supramolecular gels: Functions and uses. *Chemical Society Reviews* **2005**, *34*, 821–836, doi:10.1039/b417081b.

36. Abdallah, D. J.; Weiss, R. G. Organogels and Low Molecular Mass Organic Gelators. *Advanced Materials* **2000**, *12*, 1237–1247, doi:10.1002/1521-4095(200009)12:17<1237::AID-ADMA1237>3.0.CO;2-B.

37. Terech, P.; Weiss, R. G. Low Molecular Mass Gelators of Organic Liquids and the Properties of Their Gels. *Chemical Reviews* **1997**, *97*, 3133–3160, doi:10.1021/cr9700282.

38. Smith, D. K. Molecular Gels - Nanostructured Soft Materials. In *Organic Nanostructures*; Atwood, J. L., Steed, J. W., Eds.; Wiley-VCH Verlag GmbH & Co. KGaA, 2008 ISBN 978-3-527-31836-0.

39. Cornwell, D. J.; Smith, D. K. Expanding the scope of gels – combining polymers with low-molecular-weight gelators to yield modified self-assembling smart materials with high-tech applications. *Mater. Horiz.* **2015**, *2*, doi:10.1039/C4MH00245H.

40. Hirst, A. R.; Coates, I. a; Boucheteau, T. R.; Miravet, J. F.; Escuder, B.; Castelletto, V.; Hamley, I. W.; Smith, D. K. Low-molecular-weight gelators: elucidating the principles of gelation based on gelator solubility and a cooperative self-assembly model. *Journal of the American Chemical Society* **2008**, *130*, 9113–21, doi:10.1021/ja801804c.

41. Ananikov, V. P.; Khemchyan, L. L.; Ivanova, Y. V; Bukhtiyarov, V. I.; Sorokin, A. M.; Prosvirin, I. P.; Vatsadze, S. Z.; Medved'ko, A. V; Nuriev, V. N.; Dilman, A. D.; Levin, V. V; Koptyug, I. V.; Kovtunov, K. V; Zhivonitko, V. V; Likholobov, V. A.; Romanenko, A. V.; Simonov, P. A.; Nenajdenko, V. G.; Shmatova, O. I.; Muzalevskiy, V. M.; Nechaev, M. S.; Asachenko, A. F.; Morozov, O. S.; Dzhevakov, P. B.; Osipov, S. N.; Vorobyeva, D. V; Topchiy, M. A.; Zotova, M. A.; Ponomarenko, S. A.; Borshchev, O. V; Luponosov, Y. N.; Rempel, A. A.; Valeeva, A. A.; Stakheev, A. Y.; Turova, O. V.; Mashkovsky, I. S.; Sysolyatin, S. V.; Malykhin, V. V; Bukhtiyarova, G. A.; Terent'ev, A. O.; Krylov, I. B. Development of new methods in modern selective organic synthesis: preparation of functionalized molecules with atomic precision. *Russian Chemical Reviews* **2014**, *83*, 885–985, doi:10.1070/RC2014v83n10ABEH004471.

42. Desvergne, J.-P. Organic gelators and hydrogelators. *Beilstein Journal of Organic Chemistry* **2010**, *6*, 846–847, doi:10.3762/bjoc.6.99.

43. Smith, D. K. Molecular gels-underpinning nanoscale materials with organic chemistry. *Tetrahedron* **2007**, *63*, 7283–7284, doi:10.1016/j.tet.2007.05.026.

44. Liu, X. Y. *Low Molecular Mass Gelator*; Springer-Verlag Berlin Heidelberg: Berlin ; New York, 2005; Vol. 256; ISBN 978-3-540-25321-1.

45. Weiss, R. G.; Terech, P. *Molecular gels: Materials with self-assembled fibrillar networks*; 1st ed.; Springer Netherlands, 2006; ISBN 1402033524.

46. Jones, C. D.; Steed, J. W. Gels with sense: supramolecular materials that respond to heat, light and sound. *Chem. Soc. Rev.* **2016**, *45*, doi:10.1039/C6CS00435K.

47. Yang, H.; Yi, T.; Zhou, Z.; Zhou, Y.; Wu, J.; Xu, M.; Li, F.; Huang, C. Switchable fluorescent organogels and mesomorphic superstructure based on naphthalene derivatives. *Langmuir The Acs Journal Of Surfaces And Colloids* **2007**, *23*, 8224–8230.

48. Sahoo, P.; Sankolli, R.; Lee, H.-Y.; Raghavan, S. R.; Dastidar, P. Gel sculpture: moldable, load-bearing and self-healing non-polymeric supramolecular gel derived from a simple organic salt. *Chemistry (Weinheim an der Bergstrasse, Germany)* **2012**, *18*, 8057–63, doi:10.1002/chem.201200986.

49. Cornwell, D. J.; Okesola, B. O.; Smith, D. K. Multidomain hybrid hydrogels: Spatially resolved photopatterned synthetic nanomaterials combining polymer and low-molecular-weight gelators. *Angewandte Chemie - International Edition* **2014**, *53*, 12461–12465, doi:10.1002/anie.201405098.

50. Morris, K. L.; Chen, L.; Raeburn, J.; Sellick, O. R.; Cotanda, P.; Paul, A.; Griffiths, P. C.; King, S. M.;

O'Reilly, R. K.; Serpell, L. C.; Adams, D. J. Chemically programmed self-sorting of gelator networks. *Nature Communications* **2013**, *4*, 1–6, doi:10.1038/ncomms2499.

51. Lee, J. H.; Jung, S. H.; Lee, S. S.; Kwon, K.-Y.; Sakurai, K.; Jaworski, J.; Jung, J. H. Ultraviolet Patterned Calixarene-Derived Supramolecular Gels and Films with Spatially Resolved Mechanical and Fluorescent Properties. *ACS Nano* **2017**, *11*, 4155–4164, doi:10.1021/acsnano.7b00997.
52. Ajayaghosh, A.; Praveen, V. K.; Vijayakumar, C. Organogels as scaffolds for excitation energy transfer and light harvesting. *Chemical Society reviews* **2008**, *37*, 109–22, doi:10.1039/b704456a.
53. Okesola, B. O.; Smith, D. K. Applying low-molecular weight supramolecular gelators in an environmental setting – self-assembled gels as smart materials for pollutant removal. *Chem. Soc. Rev.* **2016**, *45*, doi:10.1039/C6CS00124F.
54. Vieira, V.; Lima, A.; de Jong, M.; Smith, D. K. Commercially-relevant orthogonal multi-component supramolecular hydrogels for programmed cell growth. *Chemistry - A European Journal* **2018**, doi:10.1002/chem.201803292.
55. Vatsadze, S. Z.; Tyurin, V. S.; Zatsman, A. I.; Manaenkova, M. A.; Semashko, V. S.; Krut'ko, D. P.; Zyk, N. V.; Churakov, A. V.; Kuz'mina, L. G. New stereoselective intramolecular redox reaction in the system of 3,7-diazabicyclo[3.3.1]nonan-9-one. *Russian Journal of Organic Chemistry* **2006**, *42*, 1225–1231, doi:10.1134/S1070428006080215.
56. Semashko, V. S.; Vatsadze, S. Z.; Zyk, N. V.; Godovikov, I. A. An NMR study of quaternary ammonium salts of 5,7-dimethyl-1,3- diazaadamantan-6-one. *Russian Chemical Bulletin* **2008**, *57*, 2207–2209, doi:10.1007/s11172-008-0303-5.
57. Balakhonov, S. V.; Vatsadze, S. Z.; Churagulov, B. R. Effect of supercritical drying parameters on the phase composition and morphology of aerogels based on vanadium oxide. *Russian Journal of Inorganic Chemistry* **2015**, *60*, 9–15, doi:10.1134/S0036023615010027.
58. Shlyakhtin, A. V.; Vatsadze, S. Z.; Krut'ko, D. P.; Lemenovskii, D. A.; Zabalov, M. V. Carboxylation of aromatic compounds in a supercritical carbon dioxide medium. *Russian Journal of Physical Chemistry B* **2012**, *6*, 818–826, doi:10.1134/S199079311207007X.
59. Sheldrick, G. M. A short history of SHELX. *Acta Crystallographica Section A: Foundations of Crystallography* 2008, *64*, 112–122.
60. Yu, G.; Yan, X.; Han, C.; Huang, F. Characterization of supramolecular gels. *Chemical Society reviews* **2013**, *42*, doi:10.1039/c3cs60080g.
61. Draper, E. R.; Adams, D. J. How should multicomponent supramolecular gels be characterised? *Chemical Society Reviews* 2018, *47*.
62. Dawn, A.; Kumari, H. Low Molecular Weight Supramolecular Gels Under Shear: Rheology as the Tool for Elucidating Structure–Function Correlation. *Chemistry - A European Journal* 2018, *24*.
63. Cui, H.; Goddard, R.; Pörschke, K. R. Degradation of dichloromethane by bispidine. *Journal of Physical Organic Chemistry* **2012**, *25*, 814–827, doi:10.1002/poc.2909.
64. Zefirov, N. S.; Palyulin, V. A. Conformational Analysis of Bicyclo[3.3.1]nonanes and Their Hetero Analogs. In *Topics in Stereochemistry*; Iliel, E. L., Wilen, S. H., Eds.; 1991; Vol. 20, pp. 171–230 ISBN 0-471-60026-1.
65. Groom, C. R.; Bruno, I. J.; Lightfoot, M. P.; Ward, S. C. The Cambridge structural database. *Acta Crystallographica Section B: Structural Science, Crystal Engineering and Materials* **2016**, *72*, 171–179, doi:10.1107/S2052520616003954.
66. Kudryavtsev, K. V.; Vatsadze, S. Z.; Semashko, V. S.; Churakov, A. V. *syn* -3-(4-Chlorobenzyl)-1,5-dimethyl-3,7-diazabicyclo[3.3.1]nonan-9-ol. *Acta Crystallographica Section E*

Structure Reports Online **2012**, *68*, o2373–o2373, doi:10.1107/S1600536812030310.

67. Maekawa, H.; Nishiyama, Y. Selective introduction of a trifluoroacetyl group onto 4-vinylpyridines through magnesium-promoted reduction. *Tetrahedron* **2015**, *71*, 6694–6700, doi:10.1016/j.tet.2015.07.046.
68. Ebead, A.; Fournier, R.; Lee-Ruff, E. Synthesis of cyclobutane nucleosides. *Nucleosides, Nucleotides and Nucleic Acids* **2011**, *30*, 391–404, doi:10.1080/15257770.2011.584513.
69. Kurkutova, E. N.; Goncharov, A. V.; Zefirov, N. S.; Palyulin, V. A. Molecular Structure of 1-Methyl-5,7-diphenyl-1,3-diazaadamantan-6-one Iodide. **1976**, *17*, 591–593.